

PENG YANG ¹, DONGDONG PANG ^{2*}

EXPERIMENTAL STUDY ON TRIAXIAL COMPRESSION MECHANICAL PROPERTIES OF GROUTING REINFORCEMENT OF BROKEN SURROUNDING ROCK

Grouting is a widely used method of reinforcement for stabilising fractured surrounding rock. To investigate the triaxial compression behaviour of surrounding rock after grouting reinforcement, laboratory-prepared grouted specimens were subjected to triaxial compression tests using an RMT-150B testing system. The analysis focused on the effects of confining stress, particle size, and water-to-cement ratio on the stress-strain behaviour. The internal friction angle and cohesion were determined based on the Mohr-Coulomb criterion. The variations in strain at peak stress and the elastic modulus were clarified, and the failure modes of the grouted specimens were examined. Additionally, Kendall's correlation analysis was employed to evaluate the relationship between confining stress and other parameters. The results indicate that increasing confining stress significantly enhances the load-bearing capacity of the surrounding rock. The optimal rock particle gradation was observed when the particle size ranged between 5-10 mm, yielding the highest compressive capacity. Conversely, increasing the water-to-cement ratio reduced the strength of the specimens. Among the analysed factors, confining stress exhibited the strongest correlation with peak stress.

Keywords: Broken surrounding rock; Triaxial compression; Peak stain; Elastic modulus

1. Introduction

Discontinuous planes are typically randomly distributed within the rock mass. However, in specific areas such as fault fracture zones, the distribution density of these discontinuous planes is significantly higher. Coupled with the loading and unloading effects induced by underground mining activities, secondary fractures frequently develop, leading to the abnormal

¹ JOINT NATIONAL-LOCAL ENGINEERING RESEARCH CENTER FOR SAFE AND PRECISE COAL MINING, ANHUI UNIVERSITY OF SCIENCE AND TECHNOLOGY, HUAINAN 232001, CHINA

² ANHUI UNIVERSITY OF SCIENCE AND TECHNOLOGY, CHINA

* Corresponding author: 793053508@qq.com



fracturing of roadway surrounding rock. To ensure the stability of fractured surrounding rock, grouting reinforcement is commonly employed to enhance its load-bearing capacity [1]. After grouting, the surrounding rock is subjected to three-dimensional stress loading (Fig. 1). In the Fig. 1, σ_z is the vertical stress, σ_x and σ_y are the horizontal stress. In this paper, the conventional triaxial test is carried out, and it is considered that σ_x and σ_y are equal. Grouting reinforcement involves injecting cement slurry or chemical slurry into the gaps between rock blocks to enhance the cementation strength between them, thereby improving the load-bearing capacity of the surrounding rock. The bearing performance of surrounding rock after grouting holds great engineering significance for the optimisation of grouting parameters.

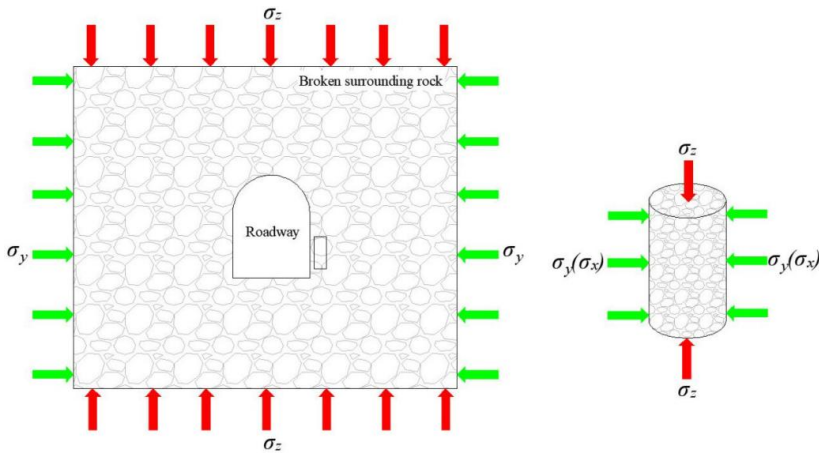


Fig. 1. Schematic diagram of grouting reinforcement of broken surrounding rock

Scholars have carried out systematic research on the mechanical properties of fractured rock mass. In 1979, J.C. Jaeger and N.J.W. Cook [2] first proposed the single structural plane theory, used two Mohr-Coulomb formulas to describe the shear failure of intact rock and along the structural plane, respectively, and established the strength model of the fractured rock mass. T. Ramamurthy and V.K. Aron [3] established the nonlinear failure criterion of rock mass and put forward the first empirical formula suitable for determining the strength of single fracture rock mass. M. Singh and B. Singh [4] concluded that when the fracture dip angle is 30° , 45° and 60° , the deformation of fractured rock mass is mainly due to the permanent deformation caused by the sliding of rock block along the fracture surface, and the elastic theory is no longer suitable. Tang et al. [5] studied the stress-strain curve, mechanical parameters and failure mode of single fracture low-strength rock samples with different dip angles and lengths. Zhou et al. [6] prepared cuboid crack specimens by mixing high-strength gypsum with water, and studied the strength, crack distribution, crack incubation and evolution law and plate cracking formation mechanism of crack specimens under unilateral limited compression. Wang et al. [7] takes sandy mudstone rock specimens with different numbers and opening cracks as the research object, the strength, deformation and failure characteristics of low-strength rock specimens are analysed. Yang et al. [8-10] systematically studied the crack expansion process of red sandstone fissure samples on the strength and deformation parameters. The above research focuses on the impact of cracks

on the strength and deformation characteristics of the surrounding rock, but the grouting effect has not been considered.

In recent years, research on grouting materials has been gradually deepened. In addition to the application of cement-based materials, organic grouting materials have many fruitful research results [11-14]. However, due to the high price of organic grouting materials and the high requirements for production conditions, cement-based grouting materials are still the dominant materials used in mines at this stage [15-20].

In situ coring is difficult due to the cutting of the structural plane, with the artificial splitting method often used to prepare fractures [21-23]. Although this method can obtain fractures, it is only a single fracture, and the development form of fractures is difficult to reflect the actual situation of rock during failure, with clear artificial traces. Therefore, rock particles were used for research. Zhang et al. [24] made coal particles with particle sizes less than 3 mm, then cemented them with superfine cement (SC) and aluminium cement (AC), and self-developed polymer foam (PF) growing material, made specimens, carried out uniaxial compression tests, and analysed their mechanical properties. Pan et al. [25-28] analysed the influence of particle size and water cement ratio on the uniaxial compressive strength of the sample and the anchorage performance with parameters of broken rock grouting. Dong et al. [29] studied the mechanical properties and instability mechanism of large-scale grouting specimens under different parameters. Wang et al. [30] investigated the effects of different particle sizes and different water-to-cement ratios on the void characteristics and mechanical properties of the broken surrounding rock grouting body. Feng et al. [31] selected broken rock mass of distinct particle sizes and injected different concentrations of cement slurry, explored the mechanical bearing mechanism of broken surrounding rock grouting and solid based on acoustic emission monitoring and DIC deformation measurement technology, and established the constitutive model of grouting and solid bearing capacity of broken surrounding rock. Wu et al. examined the effect of grouting reinforcement on the bearing capacity of fissured rock masses. The strength and deformation characteristics of the rock mass reinforced by grouting under different loading modes are analysed. Wanget al. [33] simulated the mechanical characteristics of the surrounding rock in the reclaimed rock mass. Tanet al. [34] used the discrete element method (DEM) numerical model to study the effect of particle size and arrangement on the macroscopic tensile strength of rock samples. A. Kılıc [35] studied the influence of water-to-cement ratio and other factors on the pullout force of bolt by laboratory test. Mahdi Moosavi [36] carried out the direct shear tests of Portland cement consolidation of water-to-cement ratio 0.4 and 0.5, and analyzed the characteristics of consolidation strength under different confining pressures. M. Axelsson [37] conducted a research on the coagulation mechanism and diffusion performance of cement slurry under different water-to-cement ratios.

Existing studies have significantly promoted the development of grouting reinforcement of fractured surrounding rock, but the stability of rock particles cemented with cement slurry still needs to be further studied, especially the mechanical analysis under triaxial compression. The engineering rock mass is usually in a triaxial compressive stress state, and the intermediate principal stress can enhance the strength. It is safe to consider the strength under confining stress as the strength of all minimum principal stresses. Therefore, the conventional triaxial strength criterion based on the confining stress test of cylindrical specimens is often used in engineering design [38-41].

In this study, rock blocks with varying particle sizes were used as the base material to prepare grouted specimens. Triaxial compression tests were conducted using the RMT-150B testing machine to analyse the variation in stress-strain behaviour, strength parameters, strain at peak stress, and elastic modulus under different confining stresses, water-to-cement ratios, and

particle sizes. Furthermore, the deformation and failure characteristics of the grouted specimens were thoroughly analysed. The findings of this research provide a theoretical foundation for the scientific optimisation of grouting parameters in fractured surrounding rock.

2. Test introduction

2.1. Test samples and equipment

The mineral particles are selected from the rock cores taken from the 34 mining areas of Qinan Coal Mine in Huaibei mining area (Fig. 2), and the lithology is mudstone. Firstly, the rock blocks obtained from coring are broken manually, and then the rock particles with different particle sizes are screened by a standard rock screen. During fabrication, water, mudstone particles, and cement were thoroughly mixed in the mold. During specimen fabrication, water, mudstone particles, and cement were proportioned at a mass ratio of 0.5/0.75:0.5:1. The density of all specimens was controlled within the range of 2.4–2.6 g/cm³. The mudstone used in the experiments exhibited an average uniaxial compressive strength of 64.14 MPa and an elastic modulus of 18.57 GPa. The mixture was then poured into the mold and allowed to solidify, followed by 30 days of water spray curing. After the 30-day curing period, the demolding process was initiated. Subsequently, the ends of the specimens were cut and ground to ensure the parallelism error between the upper and lower end faces ≤ 0.05 mm and the flatness of the upper and lower end faces ≤ 0.02 mm. After being fabricated into standard specimens, they were stored under natural conditions for 5 days prior to testing (Fig. 3).

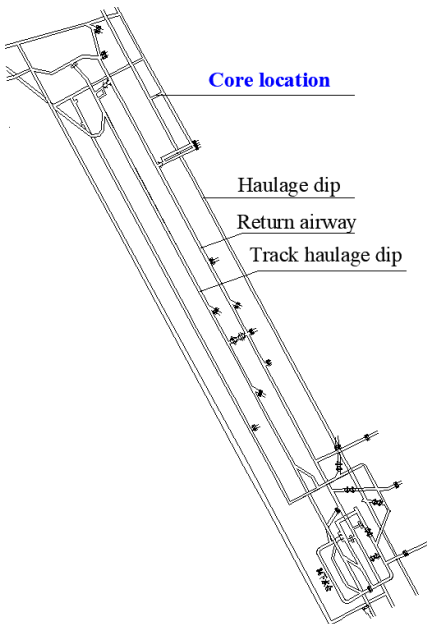


Fig. 2. The core location

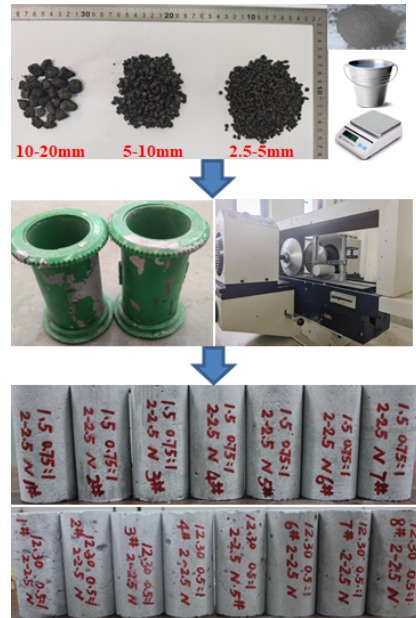


Fig. 3. Workflow of grouting specimens

2.2. Test equipment and scheme

The RMT-150B rock mechanics test system (Fig. 4) is adopted to carry out the triaxial compression test. The equipment is servo-controlled. The maximum output force of the vertical hydraulic cylinder is 1000 kN, and the maximum confining stress is 50 MPa.

Multiple groups of tests were designed and conducted to compare and analyse the effects of particle size, confining stress, and water-to-cement ratio on the strength of grouted specimens.

In the triaxial compression test, two water-to-cement ratios were used: 0.5:1 and 0.75:1. The particle sizes of the mineral particles were set at three ranges: 2.5-5 mm, 5-10 mm, and 10-20 mm. The confining stress was divided into two categories: five groups of low confining stress tests ranging from 1 MPa to 5 MPa and three groups of high confining stress tests at 11 MPa, 13 MPa, and 15 MPa. To minimize data scatter in test results, triplicate experiments were conducted for each test group. Outliers were identified and removed, with valid data subsequently selected for analysis.

The loading process consisted of two steps: **1.** The confining stress was applied to the preset value at a uniform loading rate, ensuring that pressures in both directions were synchronised in the pre-loading stage. **2.** After maintaining the confining stress at a constant level, the axial load was applied using force control mode at a rate of 0.05 MPa/s until the specimen failed in the loading failure stage. The detailed test loading path is illustrated in Fig. 5.

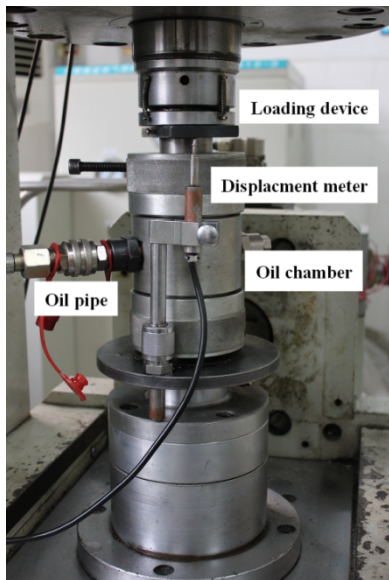


Fig. 4. Test equipment

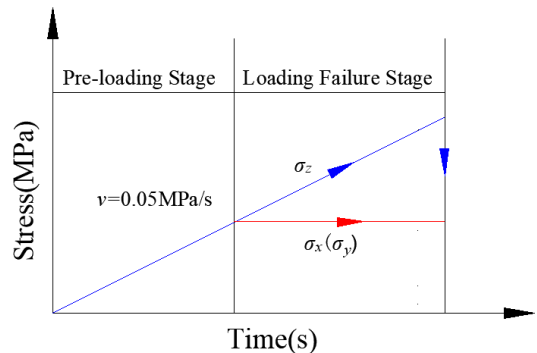


Fig. 5. Test loading path

2. Stress-strain relationship discussion

From an overall perspective, the triaxial compression stress-strain curves of the grouted specimens (Fig. 6, Fig. 7, and Fig. 8) can be categorized into two distinct types. The first type

exhibits a rising section, followed by a falling section and stabilisation, displaying particularly brittle characteristics in the post-peak stage. The second type shows no brittle drop in the post-peak stage but instead features a stress plateau, indicating ductile behaviour in the post-peak stage. The rising section before the peak is consistent across all specimens and can be divided into three stages: a nonlinear increase (fracture compaction), a linear increase (elastic stage), and another nonlinear increase (yield stage). The effects of confining stress, particle size, and water-to-cement ratio on the stress-strain curves are analysed in detail.

Fig. 6 illustrates the stress-strain curves of grouted specimens with a water-to-cement ratio of 0.5 and particle sizes of 2.5-5 mm under varying confining stresses. As the confining stress increases, the rising section of the stress-strain curve becomes progressively steeper, and the peak stress increases correspondingly. When the confining stress is below 4 MPa, the curve exhibits strain-softening behaviour. However, when the confining stress reaches 4 MPa, the post-peak stage demonstrates ductile characteristics, indicating that 4 MPa represents the transition stress from brittleness to ductility.

The deformation and failure of the specimen under axial compression – whether by splitting or shearing – are driven by tensile or shear stresses resulting from the applied compressive stress. Confining stress effectively suppresses radial deformation and delays the instability caused by the continuous expansion of deformation. When the transition stress is reached, the specimen can sustain stress at a relatively stable level. Below the transition stress, strain softening takes place; however, above that level, ductility becomes the dominant factor.

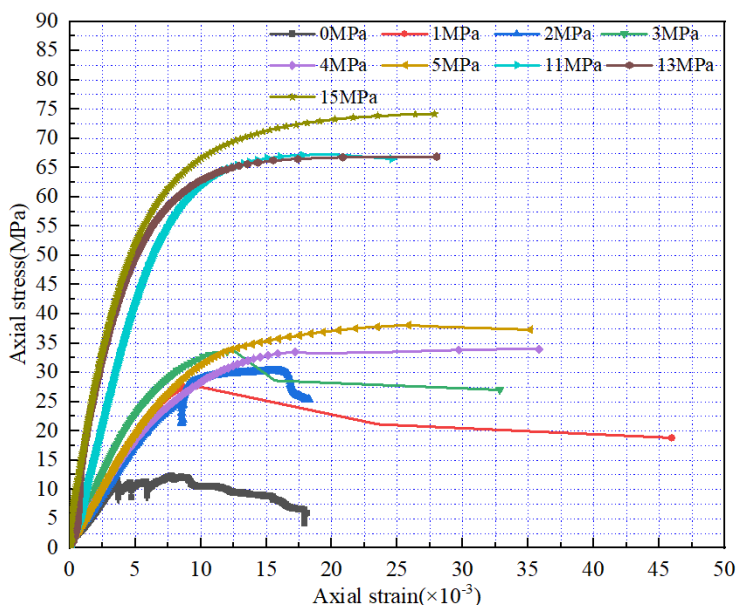


Fig. 6. Stress-strain curves under different confining stress

Additionally, Fig. 6 shows that under uniaxial compression, the stress-strain curve fluctuates around the peak. This fluctuation is attributed to the instantaneous fracture of certain rock

particles within the specimen or the sudden sliding between cement and rock particles as axial pressure increases. Higher confining stress significantly enhances shear resistance and sliding stability at the contact interfaces between rock particles and cement. As a result, these instantaneous deformations are suppressed, and the stress-strain curve becomes smoother overall.

Particle size is another critical factor influencing the performance of grouted specimens. Taking the stress-strain curve with a water-to-cement ratio of 0.5 as an example (Fig. 7), the notation “2.5-5-1” in the legend represents a particle size of 2.5-5 mm and a confining stress of 1 MPa, with similar notation for other conditions. Three confining stress levels – 1 MPa, 5 MPa, and 13 MPa – were selected for analysis, and the nine stress-strain curves were grouped into three categories based on confining stress.

When the confining stress is 1 MPa, the rising section of the stress-strain curve for specimens with a particle size of 2.5-5 mm is the slowest, while the increasing section for specimens with a particle size of 5-10 mm is the steepest. Correspondingly, the peak stress of the 5-10 mm particle size is significantly higher than that of other particle sizes. A similar trend is observed under confining stresses of 5 MPa and 13 MPa, where specimens with intermediate particle sizes exhibit higher strength and elastic modulus than small or large particle sizes. As can be seen from Fig. 7, under a confining stress of 1 MPa, the peak strains for small-, medium-, and large-particle-sized specimens are 8.7×10^{-3} , 5.7×10^{-3} , 5.1×10^{-3} , respectively, indicating that larger particle sizes result in smaller pre-peak deformations. This phenomenon may be attributed to the greater initial crack density in smaller particles, where crack closure during loading induces additional deformation. Notably, the peak strains of medium- and large-particle-sized specimens exhibit close proximity. For specimens undergoing brittle failure under 5 MPa confining stress, the peak strains are 11.1×10^{-3} (large-particle) and 10.5×10^{-3} (medium-particle), demonstrating a consistent trend with the observations at 1 MPa confining pressure.

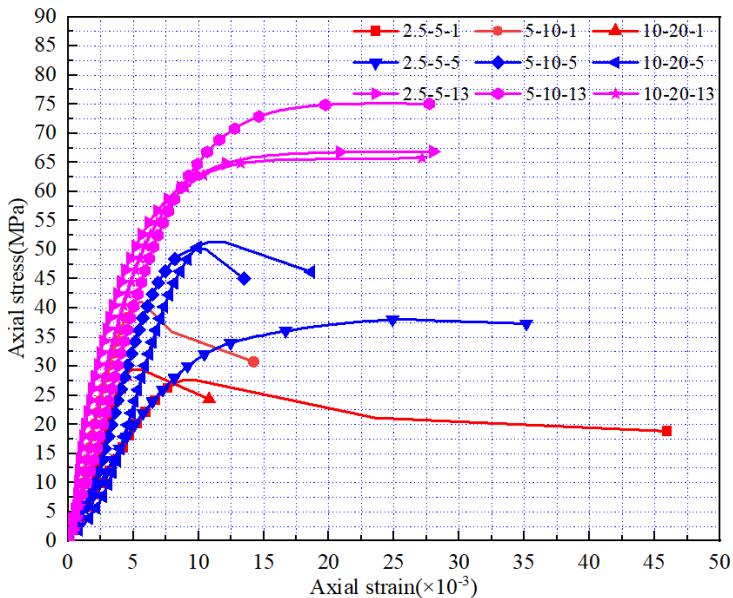


Fig. 7. Stress-strain curves of different particle sizes

This behaviour can be explained as follows: for small particle sizes, the cement slurry fills the rock particle gaps more uniformly, resulting in better structural integrity. However, the friction between particles is low, leading to reduced resistance to deformation and, thus, lower strength and elastic modulus. With larger particle sizes, the gaps between rock particles increase, allowing the cement slurry to occupy more space. Since the cement slurry has low strength, the overall strength and elastic modulus of large-particle grouted specimens remain relatively low. Specimens with intermediate particle sizes provide the best balance between structural integrity and particle friction, resulting in superior strength and elastic modulus.

Regarding deformation behaviour, when the confining stress is 1 MPa, specimens with different particle sizes exhibit brittle deformation and failure. At 13 MPa, all specimens exhibit ductile characteristics. At 5 MPa, specimens with intermediate and large particle sizes show brittle behaviour, while those with small particle sizes display ductile behaviour. This indicates that smaller particle sizes correspond to lower transition stresses from brittle to ductile behaviour.

The water-to-cement ratio is set at 0.5 and 0.75, with a particle size of 2.5-5 mm. The confining stresses are 1 MPa, 3 MPa, and 5 MPa for comparative analysis, resulting in six stress-strain curves, which are grouped into three categories (Fig. 8). The arrow in the figure indicates the change in the water-to-cement ratio from 0.5 to 0.75 under the same confining stress.

When the water-to-cement ratio increases from 0.5 to 0.75, the peak stress and elastic modulus of the specimens decrease significantly. This reduction is attributed to the higher water content causing segregation between the cement slurry and water, at the same time, high water-to-cement ratio will make the specimen produce more pores, thereby lowering the strength of the cement slurry. Furthermore, at a confining stress of 3 MPa, strain softening is observed after the peak for specimens with a water-to-cement ratio of 0.5. However, when the ratio increases to 0.75, the post-peak behaviour transitions to ductile, indicating that a higher water-to-cement ratio reduces the transformation stress from brittle to ductile behaviour.

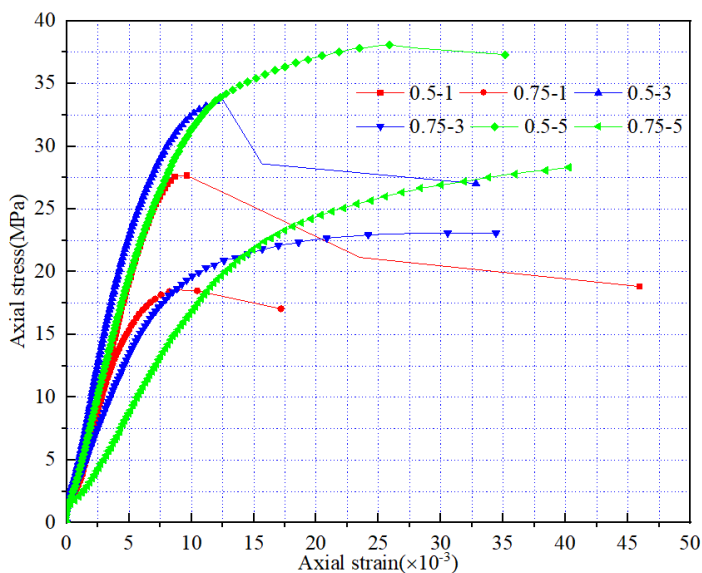


Fig. 8. Stress-strain of different water-to-cement ratio

3. Strength characteristics

3.1. Variation law of internal friction angle and cohesion

According to the Mohr-Coulomb criterion, the relationship between the principal stresses is

$$\sigma_1 = \frac{1 + \sin \varphi}{1 - \sin \varphi} \sigma_3 + \frac{2c \cos \varphi}{1 - \sin \varphi} \quad (1)$$

Where: σ_1 and σ_3 are the maximum and minimum principal stresses, respectively, (MPa); φ is the internal friction angle, ($^\circ$); c is cohesion, (MPa).

From the above formula, it can be observed that the maximum principal stress is linearly related to the minimum principal stress. When plotted on a graph (Fig. 9), the relationship can be fitted using a linear function, allowing the coefficient to be determined.

$$a = \frac{1 + \sin \varphi}{1 - \sin \varphi} \quad (2)$$

$$b = \frac{2c \cos \varphi}{1 - \sin \varphi} \quad (3)$$

The internal friction angle φ and cohesion c are then determined as:

$$\varphi = \arcsin \left[\frac{a - 1}{a + 1} \right] \quad (4)$$

$$c = b(1 - \sin \varphi) / (2 \cos \varphi) \quad (5)$$

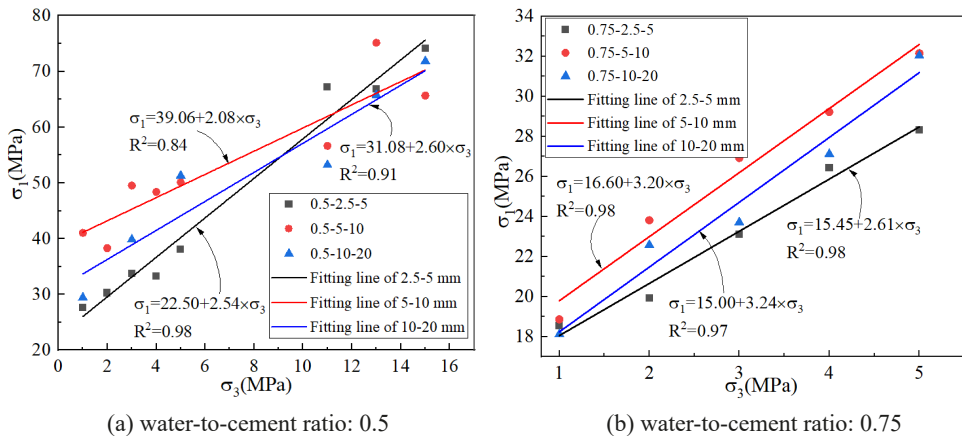


Fig. 9. Strength fitting curve under different water-to-cement ratio

According to the test results, the strength results under different particle sizes, different water-to-cement ratio and different confining pressures are shown in TABLE 1 and TABLE 2.

It should be noted that when the water-to-cement ratio is 0.5, the confining pressure data of 2 MPa and 4 MPa under the particle size of 10-20 mm are obviously abnormal, so they are not involved in the fitting. The high confining pressure test was not carried out when the water-to-cement ratio was 0.75.

TABLE 1

Different confining pressure and particle size strength (water-to-cement ratio 0.5)

Confining stress/MPa		1	2	3	4	5	11	13	15
Strength/MPa	2.5-5 mm	27.66	30.28	33.71	33.30	38.07	67.25	66.87	74.16
	5-10 mm	41.04	38.30	49.54	48.38	50.11	56.65	75.14	65.66
	10-20 mm	29.45	—	39.85	—	51.30	53.24	65.79	71.84

TABLE 2

Different confining pressure and particle size strength (water-to-cement ratio 0.75)

Confining stress/MPa		1	2	3	4	5
Strength/MPa	2.5-5 mm	18.54	19.93	23.10	26.42	28.32
	5-10 mm	18.86	23.81	26.82	29.22	32.15
	10-20 mm	18.12	22.58	23.71	27.12	32.03

Based on the fitting results, the strength parameters under different water-to-cement ratios and particle sizes were calculated using the above Eqs. (4) and (5), as presented in TABLE 1. When the water-to-cement ratio is 0.75, the internal friction angle increases gradually with the increase in particle size, showing an overall increase of 29.2%, while cohesion decreases steadily, with a reduction of 16.95%. In contrast, when the water-to-cement ratio is 0.5, the internal friction angle first decreases and then increases with increasing particle size, whereas cohesion initially increases and then decreases.

With the increase in the water-to-cement ratio, the internal friction angle increases while cohesion decreases for the same particle size. This is primarily because the strength of the cement slurry decreases as the water-to-cement ratio increases, leading to a reduction in cohesion. However, the higher water-to-cement ratio enhances the fluidity of the slurry, resulting in better penetration and distribution within the specimen. This improves the overall cementation process and structural integrity of the grouted specimen, thereby contributing to the observed increase in the internal friction angle.

TABLE 3

Strength parameters of grouting specimens

Water-to-cement ratio	Particle size	a	b /(MPa)	ϕ /(°)	c /(MPa)
0.5	2.5-5	2.54	22.5	25.8	7.06
	5-10	2.08	39.06	20.5	13.54
	10-20	2.6	31.08	26.4	9.64
0.75	2.5-5	2.61	15.45	26.5	4.78
	5-10	3.2	16.6	31.6	4.64
	10-20	3.24	15	31.9	4.17

The strength and elastic modulus of the grouted specimen are jointly influenced by cohesion and the internal friction angle. Although these two parameters exhibit different variation trends with increasing particle size, there exists an equilibrium point at the intermediate particle size where their combined effects result in the highest strength. This equilibrium explains why the strength and elastic modulus of the specimens with intermediate particle sizes are greater, as reflected in the stress-strain curves.

3.2. Variation law of ultimate strain and elastic modulus

Fig. 10 illustrates the distribution trends of peak strain and elastic modulus under varying confining stress levels for a water-to-cement ratio of 0.5 and a particle size of 2.5-5 mm. The elastic modulus is represented by the secant modulus at half of the peak stress.

In general, as the confining stress increases from 1 MPa to 15 MPa, the peak strain rises from 9×10^{-3} to 18.81×10^{-3} , representing an increase of 2.09 times. Similarly, the elastic modulus increases from 3.76 GPa to 12.88 GPa, showing an increase of 2.43 times. These results demonstrate that increasing the confining stress significantly enhances both the peak strain and the elastic modulus.

The notable improvement in peak strain indicates that the specimen exhibits better adaptability to deformation under higher confining stress, highlighting its enhanced resistance to failure in such conditions.

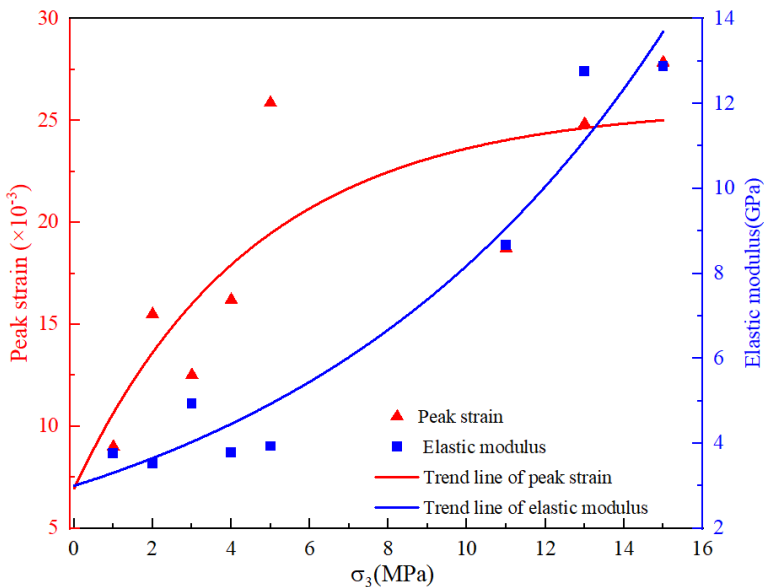


Fig. 10. Influence of confining stress (water-to-cement ratio 0.5, particle size 2.5-5 mm)

Fig. 11 illustrates the variation of peak strain and elastic modulus with particle size. When the confining stress is below 5 MPa, the peak strain initially decreases and then increases as the

particle size increases. In contrast, the elastic modulus exhibits the opposite trend. Specifically, for particle sizes of 5-10 mm, the peak strain is the lowest, while the elastic modulus is the highest. This indicates that specimens with particle sizes of 5-10 mm exhibit the best cementation, minimal internal gaps, and strong resistance to deformation.

However, when the confining stress increases to 11 MPa, the relationship between peak strain and particle size becomes chaotic and no longer follows a unified pattern. When the confining stress exceeds 13 MPa, the elastic modulus for particle sizes of 2.5-5 mm is the highest, while that for particle sizes of 5-10 mm is the lowest. These observations suggest that the effect of particle size on the mechanical properties of the specimen diminishes and becomes more complex under higher confining stresses.

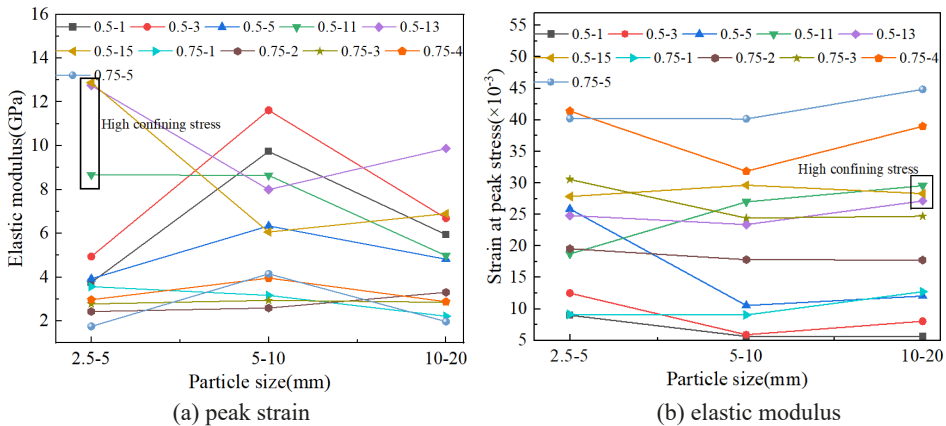


Fig. 11. Effect of particle size to peak strain and elastic modulus

The influence of the water-to-cement ratio on peak stress and elastic modulus is shown in Fig. 12, with the data corresponding to a particle size of 2.5-5 mm. As the water-to-cement ratio increases, the peak strain also increases. This is attributed to the evident separation between the cement slurry and water, leading to larger deformation under axial compression. Moreover, the rate of increase in peak strain becomes more pronounced as the confining stress rises.

At the same time, it can be observed that with an increase in the water-to-cement ratio, the elastic modulus decreases gradually. This indicates a slower stress-rise stage, which corresponds well to the observed increase in axial strain. These results highlight the negative impact of a higher water-to-cement ratio on the stiffness and resistance of the grouted specimen, particularly under increasing confining stress.

4. Failure characteristics

TABLE 2 presents the failure modes of specimens under different confining stresses, particle sizes, and water-to-cement ratios. As the confining stress increases from 1 MPa to 5 MPa, the failure mode transitions from complex modes such as splitting and shear to predominantly shear failure. At a confining stress of 1 MPa, multiple cracks are observed, whereas at 5 MPa, only

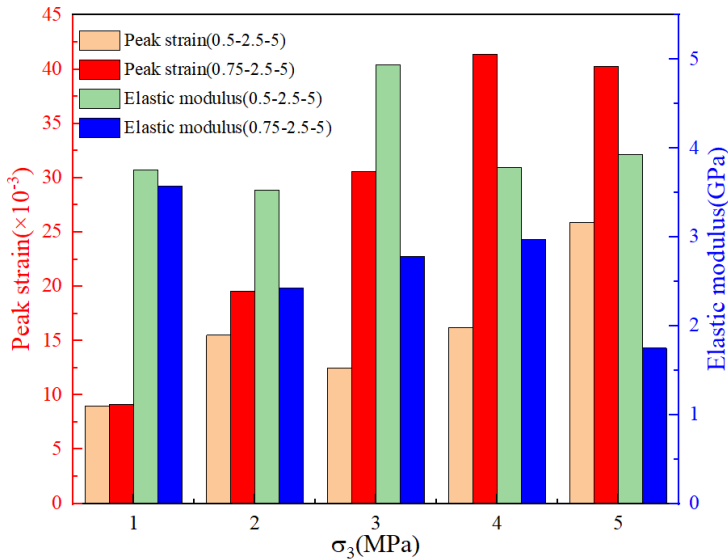


Fig. 12. Influence law of water-to-cement ratio

one primary control crack is evident. From the fracture photos, it can be seen that the mudstone particles can still remain intact when the specimen is damaged, and the damaged part is the injection matrix, because the strength of mudstone is higher than that of cement.

When the confining stress is low, the primary crack significantly influences the failure mode of the specimen. However, as the confining stress increases, the primary crack gradually closes, reducing its impact on the failure mode. Under higher confining stress, the failure mode becomes more uniform, typically forming a single or relatively regular shear plane.

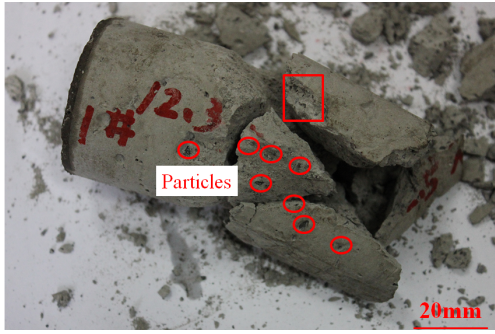
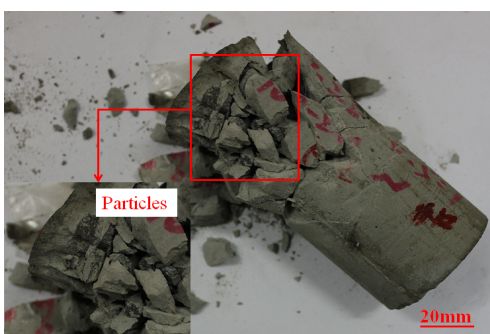
Due to the end effect, the radial expansion of the specimen is restrained near the ends, but this effect diminishes further away from the loading indenter. Consequently, the shear failure surface exhibits a conical shape, with diagonal failure dominating. The failure surface initiates and terminates on the side of the specimen rather than at the ends, reflecting the influence of axial compression and the confining stress.

When the particle size increases from 2.5-5 mm to 10-20 mm, the failure mechanism of the specimen remains consistent, exhibiting shear failure along the main control surface. Due to the end effect, the shear failure surface maintains a conical shape; however, as particle size increases, the shear failure surface becomes progressively coarser.

This coarsening is attributed to the obstruction caused by large-sized rock particles during the development of the shear surface. Although the shear stress often cannot directly fracture the rock particles, the cementation strength between the cement slurry and rock particles is typically lower than the applied shear force. As a result, the entire rock particles are displaced or detached from the specimen. The larger the rock particles, the rougher and coarser the resulting shear failure surface.

An increase in the water-to-cement ratio enhances the degree of cementation between rock particles. From the figure, it can be observed that under a confining stress of 4 MPa and a water-to-cement ratio of 0.5, the specimen with a particle size of 10-20 mm exhibits shear failure, with

Photos after the failure

confining stress 1 MPa (0.5-2.5-5)	confining stress 5 MPa (0.5-2.5-5)
	
particle size 2.5-5 mm (0.5-3)	particle size 10-20 mm (0.5-3)
	
Water-to-cement ratio 0.5 (10-20-4)	water-to-cement ratio 0.75 (10-20-4)
	

large rock particles remaining intact and not detaching after failure. However, when the water-to-cement ratio is increased to 0.75, more rock particles are observed in the damaged specimen. This occurs because the higher water-to-cement ratio weakens the cementation strength between the cement slurry and rock particles during compression failure, causing the particles to lose adhesion to the specimen and resulting in more rock particles detaching and falling off.

5. Correlation analysis

The correlation between different mechanical parameters was analysed based on the mechanical properties of grout under varying confining stresses and particle sizes, as discussed earlier. Kendall rank correlation analysis was employed for this study, as it is well-suited for small sample sizes and does not require the data to follow a normal distribution. In this paper, Kendall rank correlation analysis was utilized to examine the relationships between various mechanical parameters of grout under different confining stresses, providing a statistical basis for understanding the interdependence of these parameters.

TABLE 5

The σ_p , ε_p and E of grouting specimens under different confining stress
(water-to-cement ratio : 0.5, particle size: 2.5-5 mm)

σ_3 /MPa	σ_p /MPa	$\varepsilon_p/10^{-3}$	E /GPa
0	7.78	12.24	3.23
1	27.41	8.6	4.28
2	30.20	15.93	3.31
3	33.71	12.51	4.42
4	33.49	17.20	3.07
5	38	24.88	3.61
11	67.13	17.08	8.27
13	66.47	17.4	9.54
15	74.16	27.85	8.66

The correlation coefficient matrix, derived from the above data (TABLE 5), is a diagonal matrix that illustrates the relationships between various mechanical parameters (TABLE 6). The correlation coefficient between the peak stress of the grouting specimen and the confining stress is 0.89, indicating a strong positive correlation. This reflects the significant effect of confining stress on specimen strength, a conclusion supported by numerous studies^[42-43].

TABLE 6

Correlation coefficient matrix

	σ_3	σ_p	ε_p	E
σ_3	1	0.89	0.72	0.56
σ_p	0.89	1	0.61	0.56
ε_p	0.72	0.61	1	0.28
E	0.56	0.56	0.28	1

Additionally, the strength of the grouting specimen shows a strong positive correlation with the peak strain, with a correlation coefficient of 0.72. The correlation coefficient between confining stress and elastic modulus is 0.56, demonstrating that an increase in confining stress enhances the elastic modulus.

The correlations between confining stress, peak strain, and elastic modulus with the strength of grouting specimens are ranked as follows: confining stress > peak strain > elastic modulus.

Furthermore, the strength of the specimen exhibits strong positive correlations with both the peak strain (correlation coefficient 0.61) and the elastic modulus (correlation coefficient 0.56), highlighting the interdependence of these parameters in determining the mechanical behaviour of grouting specimens.

6. Conclusions

- (1) As the confining stress increases, the specimens transition from brittle to ductile behaviour, accompanied by increases in both peak strain and elastic modulus. The peak stress and elastic modulus reach their maximum values for specimens with particle sizes of 5-10 mm, indicating the optimal gradation. Additionally, the transformation stress increases with larger particle sizes. Conversely, as the water-to-cement ratio increases, both the peak stress and elastic modulus decrease, while the transformation stress continues to rise.
- (2) As the water-to-cement ratio increases, the cohesion of the grouting specimen initially increases and then decreases. Under different water-to-cement ratios, the variation patterns of internal friction angle and cohesion with increasing particle size differ, reflecting the complex interaction between particle size, cementation, and slurry properties.
- (3) The peak strain and elastic modulus exhibit a nonlinear increase with the rise in confining stress. Under low confining stress, the peak strain and elastic modulus reach their maximum values for specimens with intermediate particle sizes. An increase in the water-to-cement ratio leads to a higher peak strain but a reduction in elastic modulus, indicating a trade-off between deformability and stiffness.
- (4) Under low confining stress, the failure of specimens exhibits multiple modes, including splitting and shear failure. As the confining stress increases, the failure is dominated by a single shear surface, with the shear failure surface becoming relatively rough for specimens with larger particle sizes. Additionally, an increase in the water-to-cement ratio reduces the strength of the cement slurry, resulting in a greater number of detached and scattered rock particles in specimens with a high water-to-cement ratio.
- (5) The confining stress has the strongest influence on specimen strength, followed by peak strain, while the elastic modulus has a comparatively weaker correlation.

Data Availability

The data used to support the findings of this study are included in the article.

Acknowledgments

This work is supported by the National Natural Science Foundation for Young Scientists of China (No. 52304126), the Open Research Grant of the Joint National-Local Engineering Research Centre for Safe and Precise Coal Mining (No. EC2023028) and the open fund project of Key Laboratory of Safety and High-efficiency Coal Mining (No. JYBSYS2020203).

Reference

- [1] J. Niu, Z. Li, W. Gu, et al., Experimental study of split grouting reinforcement mechanism infilling medium and effect evaluation. *Sensors* **20** (11), 3008 (2020). DOI: <https://doi.org/10.3390/s20113088>
- [2] J.C. Jaeger, N.G.W. Cook, *Fundamentals of rock mechanics* 3rd, 1979 Chapman and Hall, London. DOI: <https://doi.org/10.1017/S001675680003274X>
- [3] T. Ramamurthy, V.K. Aron, Strength predictions for jointed rocks in confined and unconfined states. *International Journal of Rock Mechanics and Mining Sciences and Geomechanics Abstracts* **31** (1), 9-22 (1994). DOI: [https://doi.org/10.1016/0148-9062\(94\)92311-6](https://doi.org/10.1016/0148-9062(94)92311-6)
- [4] M. Singh, B. Singh, High lateral strain ratio in jointed rock masses. *Engineering Geology* **98** (3), 75-85 (2007). DOI: <https://doi.org/10.1016/j.enggeo.2007.11.004>
- [5] J.X. Tang, L.R. Kong, Y.L. Wang, et al., Experiment on effects of fissure dip angle and length on mechanical properties and failure modes of low-strength rock mass. *Industrial Construction* **49** (2), 85-92 (2019). DOI: <https://doi.org/10.1016/j.engfracmech.2018.04.044>
- [6] Y. Zhou, Z. Sun, L. Wang, et al., Meso research on mechanical properties and slab failure mechanism of pre-fractured rock mass under the condition of one side restriction loading. *Rock and Soil Mechanics* **39** (12), 4385-4394 (2018). DOI: <https://doi.org/10.16285/j.rsm.2017.2597>
- [7] Y.L. Wang, J.X. Tang, Z.Y. Dai, et al., Effect of fracture number and aperture on mechanical properties and failure modes of low-strength rock mass. *Journal of China Coal Society* **43** (12), 3338-3347 (2018). DOI: <https://doi.org/10.13225/j.cnki.jccs.2018.0365>
- [8] S.Q. Yang, Crack coalescence behavior of brittle sandstone samples containing two coplanar fissures in the process of deformation failure. *Engineering Fracture Mechanics* **78** (17), 3059-3081 (2011). DOI: <https://doi.org/10.1016/j.engfracmech.2011.09.002>
- [9] S.Q. Yang, X.G. Liu, H.W. Jing, Experimental investigation on fracture coalescence behavior of red sandstone containing two unparallel fissures under uniaxial compression. *International Journal of Rock Mechanics and Mining Sciences* **63**, 82-92 (2013). DOI: <https://doi.org/10.1016/j.ijrmms.2013.06.008>
- [10] S.Q. Yang, Study of strength failure and crack coalescence behavior of sandstone containing three pre-existing fissures. *Rock and Soil Mechanics* **34** (1), 31-39 (2013). DOI: <http://ytlx.whrsm.ac.cn/en/y2013/v34/11/31>
- [11] K. Hou, S. Wang, S. Yao, et al., Research progress on modification of polyurethane grouting materials in mines. *Coal Science and Technology (Peking)* **50**, 28-34 (2022). DOI: <https://doi.org/10.13199/j.cnki.cst.2021-0501>
- [12] C. Zhang, W. Pan, J. Wang, et al., Research Progress of the Cell Structure Characteristics and Compressive Properties of Polyurethane Foam Grouting Rehabilitation Materials. *Cailiao Daobao/Materials Reports* **38**, 3 (2024). DOI: <https://doi.org/10.11896/cldb.22070007>
- [13] X.M. Guan, H.B. Zhang, Z.P. Yang, et al., Research of high performance inorganic-organic composite grouting materials. *Journal of China Coal Society* **45** (3), 902-910 (2020). DOI: <https://doi.org/10.13225/j.cnki.jccs.SJ20.0117>
- [14] J.J. Zeng, H.Z. Li, D.D. Wei, et al., Preparation and properties of acrylate grouting material used in coal mine. *Coal Geology and Exploration* **51** (6), 22-29 (2023). DOI: <https://doi.org/10.12363/issn.1001-1986.22.10.0770>
- [15] S. Liu, G. Xie, S. Wang, Effect of curing temperature on hydration properties of waste glass powder in cement-based materials. *Journal of Thermal Analysis and Calorimetry* **119** (1), 47-55 (2015). DOI: <https://doi.org/10.1007/s10973-014-4095-6>
- [16] N.H. Mohammed, R. Pusch, N. Alansari, et al., Proportioning of cement-based grout for sealing fractured rock-use of packing models. *Engineering* **5** (10), 765-774 (2013). DOI: <https://doi.org/10.4236/eng.2013.510092>
- [17] M. Mollamahmutoğlu, E. Avci, Ultrafine portland cement grouting performance with or without additives. *KSCE Journal of Civil Engineering* **19** (7), 2041-2050 (2015). DOI: <https://doi.org/10.1007/s12205-014-1445-7>
- [18] E. Avci, M. Mollamahmutoğlu, Ucs properties of superfine cement-grouted sand. *Journal of Materials in Civil Engineering* **28** (12), 06016015 (2016). DOI: [https://doi.org/10.1061/\(ASCE\)MT.1943-5533.0001659](https://doi.org/10.1061/(ASCE)MT.1943-5533.0001659)

- [19] E. Avci, M. Mollamahmutoğlu, Permeability characteristics of superfine cement-grouted sand. *Aci Materials Journal* **114** (1), 21-28 (2017). DOI: <https://doi.org/10.14359/51689471>
- [20] W.T. Liu, H.F. Wu, J.J. Shen, Based on Box-Behnken method superfine cement grouting material ratio and performance optimization model. *Coal Science and Technology (Peking)* **52** (8), 146-158 (2024). DOI: <https://doi.org/10.12438/cst.2023-1391>
- [21] Q.S. Liu, G.F. Lei, C.B. Lu, et al., Experimental study of grouting reinforcement influence on mechanical properties of rock fracture. *Chinese Journal of Rock Mechanics and Engineering* **36** (Supp. 1), 3140-3147 (2017). DOI: <https://doi.org/10.13722/j.cnki.jrme.2016.0459>
- [22] Q.S. Liu, Y.S. Zhou, C.B. Lu, et al., Experimental study on mechanical properties of mudstone fracture before and after grouting. *Journal of Mining and Safety Engineering* **33** (3), 509-514 (2016). DOI: <https://doi.org/10.13545/j.cnki.jmse.2016.03.020>
- [23] Y.L. Lu, M.Q. He, W.S. Li, et al., Micromechanical mechanisms of grouting reinforcement in rock joints and microstructure optimization of grout-rock bonding planes. *Chinese Journal of Rock Mechanics and Engineering* **39** (9), 1808-1818 (2020). DOI: <https://doi.org/10.13722/j.cnki.jrme.2020.0302>
- [24] J.X. Zhang, Y.N. Sun, Experimental and Mechanism Study of a Polymer Foaming Grouting Material for Reinforcing Broken Coal Mass. *Material for Reinforcing Broken Coal Mass* **23** (1), 346-355 (2018). DOI: <https://doi.org/10.1007/s12205-018-0780-5>
- [25] R. Pan, Q. Wang, B. Jiang, et al., Failure of bolt support and experimental study on the parameters of bolt-grouting for supporting the roadways in deep coal seam. *Engineering Failure Analysis* **80**, 218-233 (2017). DOI: <https://doi.org/10.1016/j.engfailanal.2017.06.025>
- [26] R. Pan, Study on bolt grouting mechanism and control technology of broken surrounding rock in deep roadway. *Chinese Journal of Rock Mechanics and Engineering* **40**, 864 (2021). DOI: <https://doi.org/10.13722/j.cnki.jrme.2020.1039>
- [27] R. Pan, L. Wang, H.X. Huang, et al., Experimental study on anchorage performance and parameters of grouting anchor cable under broken surrounding rock. *Journal of Mining and Safety Engineering* **39**, 1108-1115 (2022). DOI: <https://doi.org/10.13545/j.cnki.jmse.2021.0554>
- [28] R. Pan, L. Wang, Experimental study on the bearing behavior of bolted and grouted broken surrounding rock of deep roadways in a coal mine. *KSCE Journal of Civil Engineering* **28**, 4032-4040 (2024). DOI: <https://doi.org/10.1007/s12205-024-0018-7>
- [29] H.J. Dong, J.S. Zhang, H.Y. Yao, et al., Mechanical properties and instability mechanism of large-scale grouting specimens with different parameters. *Journal of China University of Mining and Technology* **50** (1), 79-89 (2021). DOI: <https://doi.org/10.13247/j.cnki.jcumat.001233>
- [30] Q. Wang, L. Wang, B.H. Liu, et al., Study on the void characteristics and mechanical properties of the grouting body of the crushed surrounding rock. *Journal of China University of Mining and Technology* **48**, 1197-1205 (2019). DOI: <https://doi.org/10.13247/j.cnki.jcumat.001074>
- [31] G.R. Feng, J.K. Ma, Z. Li, et al., Bearing characteristics and damage mechanism of grouting reinforced body for broken surrounding rock. *Journal of the China Coal Society* **48**, 411-423 (2023). DOI: <https://doi.org/10.13225/j.cnki.jccs.2022.1265>
- [32] X.K. Wu, G.M. Zhao, X.R. Meng, et al., Load-bearing characteristics and energy evolution of fractured rock masses after granite and sandstone grouting. *Journal of Central South University* **31**, 2810-2825 (2024). DOI: <https://doi.org/10.1007/s11771-024-5760-y>
- [33] P. Wang, Y.J. Zhu, W.J. Yu, et al., Test analysis of partial compaction mechanical characteristics of weak broken surrounding rock. *Rock and Soil Mechanics* **40** (7), 2703-2712 (2019). DOI: <https://doi.org/10.16285/j.rsm.2018.0460>
- [34] X. Tan, Y.G. Hu, X. Yin, et al., Macro-micro scale tensile strength correlations for particle-dem based rock models. *Chinese Journal of Theoretical and Applied Mechanics* **56**, 1411-1425 (2024). DOI: <https://doi.org/10.6052/0459-1879-23-487>
- [35] A. Kilic, E. Yasar, A.G. Celik, Effect of grout properties on the pull-out load capacity of fully grouted rock bolt. *Tunnelling and Underground Space Technology* **17**, 355-362 (2002). DOI: [https://doi.org/10.1016/s0886-7798\(02\)00038-x](https://doi.org/10.1016/s0886-7798(02)00038-x)
- [36] Mahdi Moosavi, William F. Bawden, Shear strength of Portland cement grout. *Cement & Concrete Composites* **25**, 729-735 (2003). DOI: [https://doi.org/10.1016/S0958-9465\(02\)00101-4](https://doi.org/10.1016/S0958-9465(02)00101-4)

- [37] M. Axelsson, G. Gustafson, A. Fransson, Stop mechanism for cementitious grouts at different water cement ratios, *Tunnelling and Underground Space Technology* **24**, 390-397 (2009).
DOI: <https://doi.org/10.1016/j.tust.2008.11.001>
- [38] J.C. Jaeger, N.G.W. Cook, Robert Zimmerman, *Fundamentals of rock mechanics* 4th, 2007 Wiley-Blackwell, New York. DOI: <https://doi.org/10.1017/CBO9780511735349>
- [39] M.Q. You, Three independent parameters to describe conventional triaxial compression strength of intact rocks. *Journal of Rock Mechanics and Geotechnical Engineering* **2** (4), 350-356 (2010).
DOI: <https://doi.org/10.3724/SP.J.1235.2010.00350>
- [40] M.Q. You, Comparison of the accuracy of some conventional triaxial strength criteria for intact rock. *International Journal of Rock Mechanics and Mining Sciences* **48** (5), 852-863 (2011).
DOI: <https://doi.org/10.1016/ijrmms.2011.05.006>
- [41] M.Q. You, Effect of confining stress on Elastic modulus and relationship between fracture friction. *Geotechnical Mechanics* **24** (2), 167-170 (2003).
- [42] M.H. Li, G.Z. Yin, J. Xu, et al., A novel true-triaxial apparatus to study the geomechanical and fluid Flow aspects of energy exploitations in geological formations. *Rock Mechanics and Rock Engineering* **49**, 4647-4659 (2016).
DOI: <https://doi.org/10.1007/s00603-106-1060-7/>
- [43] G.Z. Yin, M.H. Li, J. Xu, et al., A new multi-functional true triaxial fluid-solid coupling experiment system and its applications. *Chinese Journal of Rock Mechanics and Engineering* **34** (12), 2436-2445 (2015).
DOI: <https://doi.org/10.13722/j.cnki.jrme.2015.0050>